Available online at www.sciencedirect.com
ScienceDirect
Trans. Nonferrous Met. Soc. China 28(2018) 96−102
Transactions of Nonferrous Metals Society of China
www.tnmsc.cn

Microstructures and properties in surface layers of Mg−6Zn−1Ca magnesium alloy laser-clad with Al−Si powders

Xiao-lin ZHANG[1], Ke-min ZHANG[1], Jian-xin ZOU[2]

1. School of Materials Engineering, Shanghai University of Engineering Science, Shanghai 201620, China;
2. National Engineering Research Center of Light Alloys Net Forming, School of Materials Science and Engineering, Shanghai Jiao Tong University, Shanghai 200240, China

Received 4 August 2016; accepted 19 December 2016

Abstract: Laser surface cladding with Al−Si powders was applied to a Mg−6Zn−1Ca magnesium alloy to improve its surface properties. The microstructure, phase components and chemical compositions of the laser-clad layer were analyzed by using X-ray diffractometry (XRD), scanning electron microscopy (SEM) and energy dispersive spectrometry (EDS). The results show that the clad layer mainly consists of α-Mg, Mg_2Si dendrites, $Mg_{17}Al_{12}$ and Al_3Mg_2 phases. Owing to the formation of Mg_2Si, $Mg_{17}Al_{12}$ and Al_3Mg_2 intermetallic compounds in the melted region and grain refinement, the microhardness of the clad layer ($HV_{0.025}$ 310) is about 5 times higher than that of the substrate ($HV_{0.025}$ 54). Besides, corrosion tests in the NaCl (3.5%, mass fraction) water solution show that the corrosion potential is increased from −1574.6 mV for the untreated sample to −128.7 mV for the laser-clad sample, while the corrosion current density is reduced from 170.1 to 6.7 μA/cm^2. These results reveal that improved corrosion resistance and increased hardness of the Mg−6Zn−1Ca alloy can be both achieved after laser cladding with Al−Si powders.
Key words: laser cladding; Mg−6Zn−1Ca alloy; microstructure; hardness; corrosion resistance

1 Introduction

As promising lightweight materials, magnesium alloys have been widely used in many fields, such electronic, automotive and aerospace industries, due to their high specific strength and low density [1,2]. Besides, magnesium alloys have many other advantages, such as excellent machinability, good castability, hot formability and recyclability. However, magnesium alloys also suffer from some disadvantages. For example, magnesium alloys have low hardness, poor wear and corrosion resistance, which greatly limit their further applications in industries [3,4]. Considering that these shortcomings are always related to the surface states, different surface treatment methods, such as physical and chemical depositions, micro-arc oxidation, laser cladding, painting, and ion implantation, have been applied to magnesium alloys in order to improve their surface properties [5−11].

As one of the efficient surface treated techniques, laser treatment has been widely utilized to process many kinds of metals and alloys [12−15]. The advantages of laser surface treatment include thick treated layer, fine microstructure, good metallurgical bonding with substrate, etc. In particular, fiber laser shows better application performances than CO_2 laser with high output power, high conversion efficiency, high beam quality and stable power. HAZRA and MONDAL [14] revealed that the wear resistance of the MRI 153M magnesium alloy was improved by an order of magnitude after laser cladding with Al+Al_2O_3. However, the corrosion resistance of the alloy was deteriorated owing to the presence of cracks and pores in the clad layer. TAN et al [16] have investigated the laser cladding of an AZ80 Mg alloy with Al−Cu−Zn powders under water cooling conditions. The results showed that the laser-clad layer had higher microhardness and wear/corrosion resistances of the alloy were significantly improved as a result of the formation of Al-based amorphous−nanocrystalline composite coatings. WANG and LI [17] reported that wear and corrosion resistances

Foundation item: Project (2016YBF0701205) supported by the National Key Research and Development Program of China; Projects (51271121, 51471109) supported by the National Natural Science Foundation of China; Project (13KY0501) supported by Shanghai University of Engineering Science Innovation Fund for Graduate Students, China
Corresponding author: Ke-min ZHANG; Tel: +86-21-67791198; E-mail: zhangkm@sues.edu.cn
DOI: 10.1016/S1003-6326(18)64642-4

of the AZ91HP magnesium alloy were improved by laser surface cladding with eutectic-based Ti−Ni−Al alloy. These results showed the high potential of laser surface treatments on improving surface properties of Mg alloys.

Mg−Zn−Ca ternary alloys are considered as good heat-resistance materials and bio-medical materials. Previous investigations on Mg−Zn−Ca ternary alloys mainly focused on microstructural characterizations, aging behaviors [2] and corrosion behaviors in Hank's solution [18,19]. However, the effects of surface modifications on microstructure and properties of Mg−Zn−Ca ternary alloys were not well studied. In this work, the laser surface cladding was firstly applied to a Mg−6Zn−1Ca magnesium alloy by using a fiber laser apparatus. In previous works, laser cladding with Al−Si powders was proven to be able to improve significantly the surface properties of Mg-based alloys and composites [20,21]. By considering this, the effects of the scanning speed on the microstructure, microhardness and corrosion resistance of a Mg−6Zn−1Ca alloy laser-clad with Al−Si powders were carefully investigated.

2 Experimental

2.1 Sample preparation

In the present work, the selected substrate material is the Mg−6Zn−1Ca Mg alloy, which contains about 6% Zn and 1% Ca (mass fraction). The thickness and diameter of the cylinder specimens are 10 and 35 mm, respectively. In order to obtain a clean and smooth surface, these specimens were all ground with 800-grit SiC sand paper and washed with ethanol before laser cladding. For the laser cladding treatments, the powders used in this work are commercial pure aluminum (≥99% purity) and silicon (≥99% purity) powders. Their average particle size is 75 μm. The two kinds of powders were mixed through ball-milling for 6 h with an Al to Si mass ratio of 3:1 [22]. In the end, the mixed powder was put on the substrate surface and compressed to a thickness of about 0.5 mm.

The laser cladding treatments were carried out using an IPG−YLS−5000W fiber laser (wavelength of (1075±5) nm) with the maximum output power of 5000 W. The beam is quadrate with a size of 5 mm × 5 mm and the laser cladding process was done under an argon shielding gas of 20 L/min. The scanning rate ranges from 4 to 6 mm/s with a fixed output power of 2500 W.

2.2 Microstructure analyses

In order to observe the morphology and the microstructure of the laser-clad layer from top surface to the bottom of the clad layers, the treated specimens were cut perpendicular to the scanning direction. After that, the cross sections of the specimens were ground and polished with diamond paste down to 2.5 μm. Then, the samples were cleaned with pure ethanol. In the end, the cleaned specimens were etched by an alcohol + nitric acid (volume ratio of 96:4) solution and completely dried in air. An AS−3400 scanning electron microscope (SEM) equipped with energy dispersive spectrometer (EDS) was used to examine the microstructure and compositions of the laser-clad layers. X-ray diffraction (XRD) measurements were carried out using a Shimadzu D−6000 goniometer equipped with a Cu K_α radiation source to detect the phase components in the surface of the laser-clad layers.

2.3 Surface properties

A HXD−1000 microhardness tester with Vickers indenter was used to measure the microhardness of the laser-clad specimens from the cross sections. The measurements were done with a load of 0.25 N and the loading time was set to be 15 s ($HV_{0.025}$/15). The cross section microhardness profiles were obtained by doing at least five parallel measurements at certain depth and getting the average value.

The potentiodynamic polarization measurements were performed in a standard three-electrode cell using a saturated calomel electrode as a reference electrode. Before the corrosion test, the surfaces of specimens were ground and polished with diamond paste to 2.5 μm and cleaned in pure ethanol. The corrosion tests were carried out in a 3.5% NaCl (mass fraction) water solution. The exposed area for the corrosion measurements was about 0.25 cm^2. The temperature of the solution was kept at room temperature. The potentiodynamic polarization curves were measured with a scanning rate of 0.001 mV/s. The cathodic polarization scanning started from −1872 mV (vs SCE) for the Mg−6Zn−1Ca magnesium alloy and from −500 mV (vs SCE) for the laser-clad specimens. The samples were dipped into the NaCl solution until a steady corrosion potential was achieved, and then the anodic polarization scanning was started. Afterward, the polarization curves were used to evaluate the corrosion current density (J_{corr}) and the corrosion potential (φ_{corr}) by Tafel extrapolation.

3 Results and discussion

3.1 XRD analysis

Figure 1 shows the X-ray diffraction patterns of the untreated sample and the laser-clad samples with different scanning speeds. The untreated Mg−6Zn−1Ca alloy contains α-Mg as the majority phase and Mg_2Zn and $Ca_2Mg_6Zn_3$ as the minority phases, as shown in Fig. 1. The XRD results also indicate that the clad layers are mainly composed of α-Mg and some intermetallic

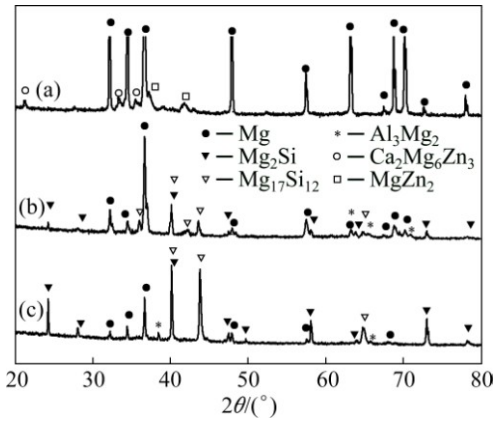

Fig. 1 XRD patterns of initial sample (a) and laser-clad sample ((b) 2500/6; (c) 2500/4)

compounds, such as $Mg_{17}Al_{12}$, Mg_2Si, and a small amount of Al_3Mg_2 phase [23]. The comparison of the peak intensity reveals that the volume fraction of $Mg_{17}Al_{12}$ and Mg_2Si phases in the surface of the sample laser-clad at 4 mm/s is higher than that of the coating obtained at 6 mm/s. This is due to the fact that more Mg from substrate is melted and involved in chemical reactions between Mg−Al and Mg−Si in the laser-clad layer when the scanning speed is lower.

3.2 Microstructure and composition analyses

To reveal the phases generated in the clad layer and their morphology, SEM and EDS analyses were carried out on the treated specimens. The typical SEM image taken in top surface layer of the laser-clad sample with the scanning speed of 6 mm/s is shown in Fig. 2, together with the elemental distribution maps of Si, Al, Mg, Zn and Ca. SEM image of Fig. 2 shows that many irregular shaped segregates present in the laser-clad layer with size ranging from several to 10 μm. The elemental distribution maps indicate that Mg is quite homogeneously distributed in the clad layer with fairly low contents of Zn and Ca, while the distributions of elements Si and Al are not homogeneous. A comparison

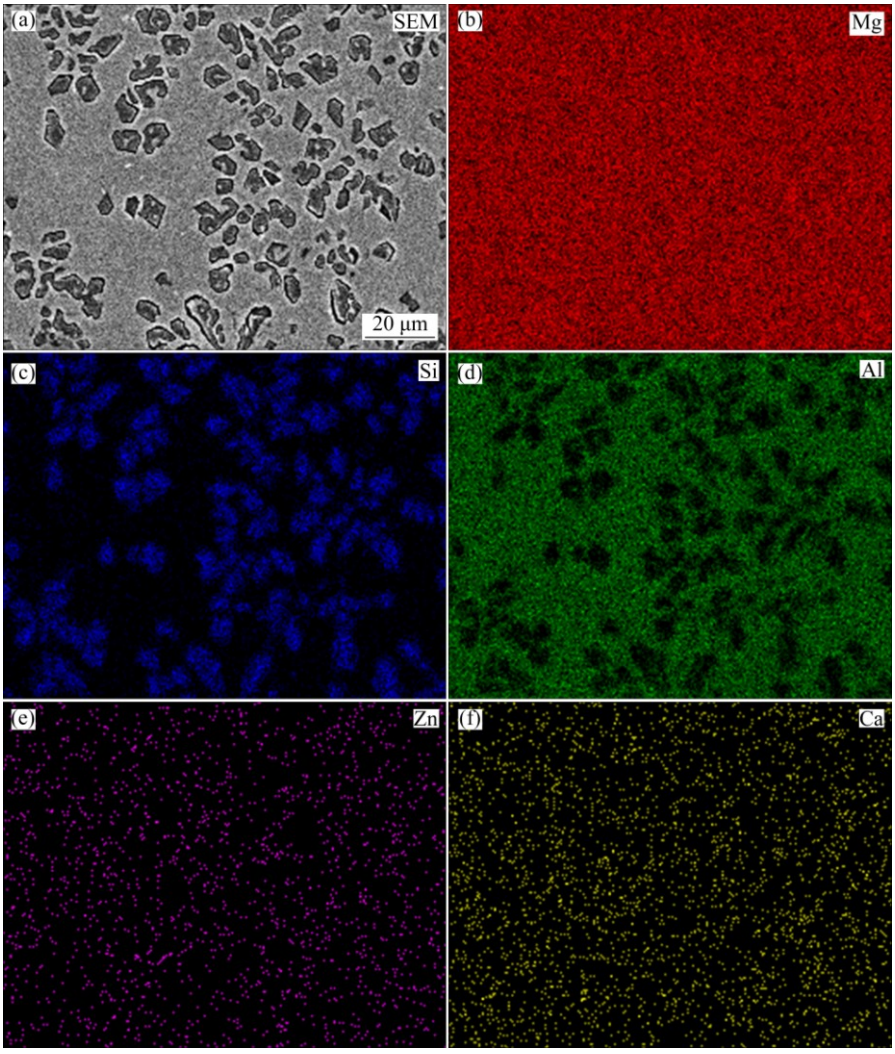

Fig. 2 SEM image of laser-clad sample with scanning speed of 6 mm/s (a) and elemental mappings of Mg (b), Si (c), Al (d), Zn (e) and Ca (f)

between SEM image and the elemental distribution maps reveals that those segregates are rich in Si but lean in Al, which should correspond to the Mg_2Si phase.

Figure 3 shows the SEM images of laser-clad samples at regions from the top surface to the melt/substrate interface. Figures 3(a) and (d) show the SEM images taken in the top surface of the samples treated with scanning speeds of 4 and 6 mm/s, respectively. They present similar morphology: segregates or dendrites distribute quite homogeneously on the matrix. In Figs. 3(b) and (d), those marked points are analyzed using EDS technique, and Table 1 gives the molar fractions of these tested points. Combining the X-ray diffraction results with the EDS results, we can conclude that in the top surface of the laser-clad layer, those dendrites or segregates are Mg_2Si, as marked by Point 1 in Fig. 3(d). While the matrix, marked as Point 2, contains Mg and $Mg_{17}Al_{12}$ and Al_3Mg_2 compounds. In the middle of the clad layer with the scanning speed of 4 mm/s, as shown in Fig. 3(b), Point *A* presents Mg_2Si phase, while Point *B* presents Al_3Mg_2 phase and Point *C* is the eutectic structure of α-Mg+$Mg_{17}Al_{12}$. Similarly, Fig. 3(d) exhibits the eutectic microstructure in the middle of sample laser-clad with the scanning speed of 6 mm/s. Figures 3(c) and (f) show that a good metallurgical bonding is generated between the composite coating and the substrate. Due to different cooling speeds and compositions in different regions, the morphology and the content of different phases are quite different from top to the bottom of the laser-clad layer. It is observed in this work that, the phase components and microstructure in the top of the clad layers are similar regardless of the scanning speed, while the microstructure and the morphology are quite different in the middle and interface area when the scanning speed changes, as shown in Fig. 3.

3.3 Microhardness

Figure 4 shows the microhardness profiles measured in the cross sections of the laser-clad samples with different scanning speeds. According to the curves shown in Fig. 4, the microhardness distribution along the depth has the similar trend for the two clad samples. The microhardness reaches the maximum value ($HV_{0.025}$ 310

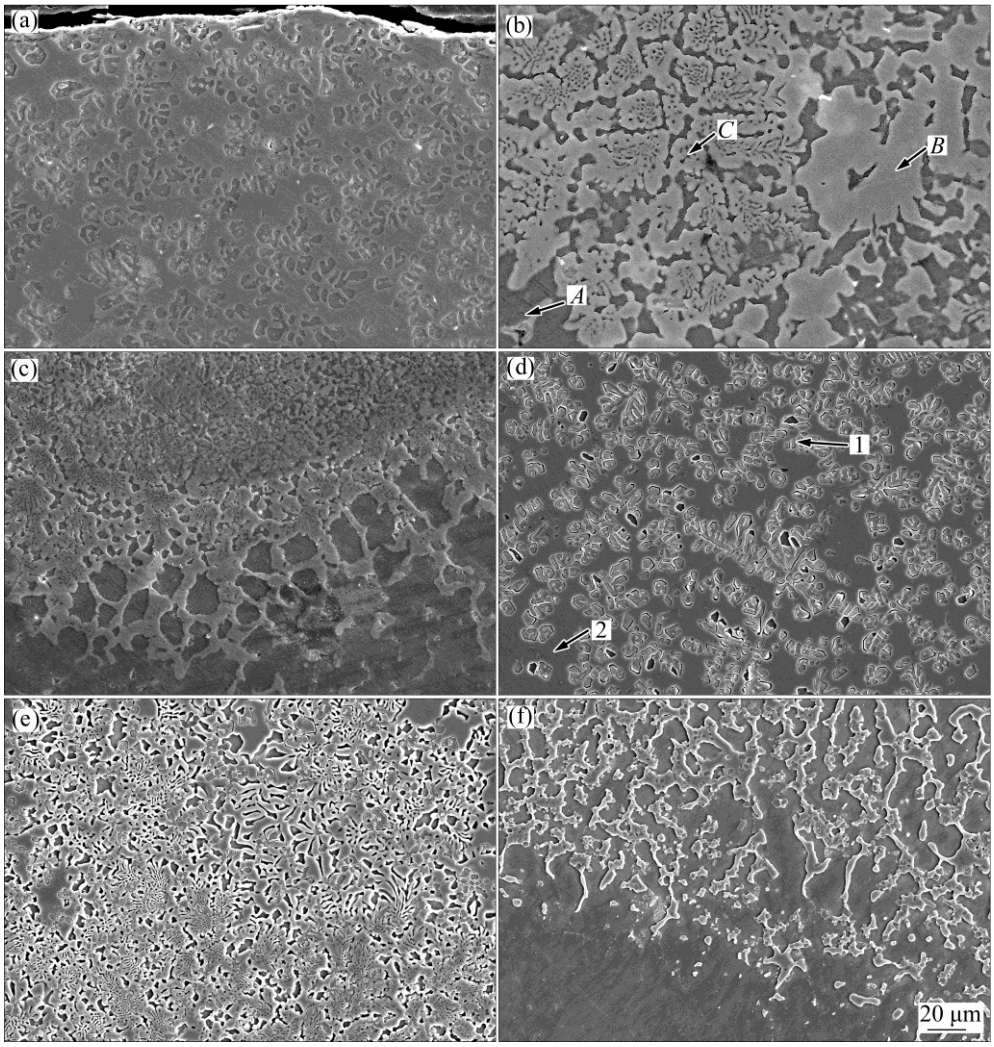

Fig. 3 SEM images taken from cross sections of laser-clad samples with scanning speeds of 4 mm/s (a−c) and 6 mm/s (d−f)

Table 1 EDS analysis results of different points marked in Fig. 3(b) and Fig. 3(d)

Position	x(Mg)/%	x(Al)/%	x(Si)/%	x(Zn)/%
A	65.23		34.77	
B	58.74	37.76		3.5
C	66.07	30.66		3.27
1	63.75	2.62	33.63	
2	47.60	49.23		2.55

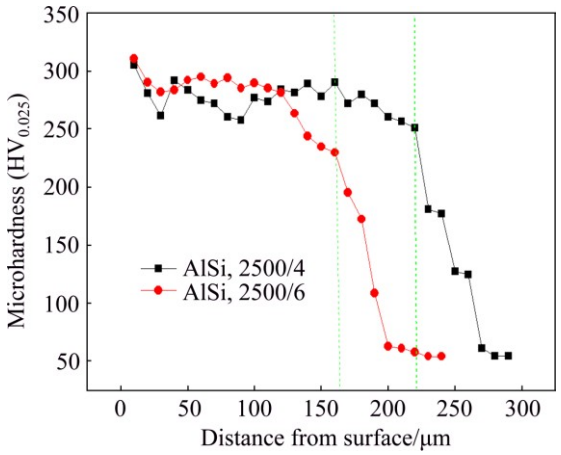

Fig. 4 Cross-section microhardness profiles of laser-clad samples with different scanning speeds

for the sample treated with 6 mm/s) in the top of laser-clad layer. It slightly decreased from the top surface to near surface region (about 30 μm from the surface). Then, after a plateau zone in the melted layer, the hardness rapidly decreases at the melt/substrate interface zone and reaches the value for the substrate (about $HV_{0.025}$ 54). Even though the grain refinement has a positive effect on increasing the hardness of the laser-clad layer, the increment in hardness of the melted zone may mainly be attributed to the formation of intermetallic compounds, such as Mg_2Si, $Mg_{17}Al_{12}$ and Al_3Mg_2 [24]. In addition, it is seen that the thickness of the melted zone increases by more than 50 μm when the laser scanning speed decreases from 6 to 4 mm/s. As is known, if the laser power is fixed, more heat energy will be absorbed by the clad layer and the substrate below when the scanning speed is low, which favors the formation of new phases containing Mg as more substrate is melted and involved in the metallurgical reactions occurred in the clad layer.

3.4 Corrosion performance

Figure 5 shows the potentiodynamic polarization curves of the initial and the laser-clad samples. The corrosion potential (φ_{corr}) and the corrosion current density (J_{corr}) calculated from Fig. 5 are listed in Table 2. According to the obtained results, the value of φ_{corr} for the two laser-clad specimens is both nobler than that of the substrate, reaching −165 mV for the laser-clad sample with the scanning speed of 4 mm/s. In addition, the J_{corr} value of the laser-clad specimen with the scanning speed of 4 mm/s is 6.7 μA/cm^2, which is only 1/25 of the untreated sample (170.1 μA/cm^2). Clearly, after the laser cladding treatment, the corrosion resistance of the specimens has been significantly improved. According to the microstructure and composition analyses shown before, the reasons for the improved corrosion resistance are as follows: Firstly, the enhanced corrosion resistance can be ascribed to the formation of an Al-rich layer on the Mg alloy surface during the laser cladding process; Secondly, the previous work done by LUNDER et al [25] demonstrated that the $Mg_{17}Al_{12}$ phase was inert to the chloride solution and was a highly corrosion resistance phase compared with Mg; Thirdly, the grain refinement induced by laser cladding also have a positive contribution to the corrosion resistance property [26]. In addition, by comparison of the corrosion potential and the corrosion current density of the two laser-clad specimens, it can be found that the sample treated at the scanning speed of 4 mm/s exhibits higher φ_{corr} and lower J_{corr} than those of the sample obtained at 6 mm/s. Such a difference can be attributed to the formation of more intermetallic compound $Mg_{17}Al_{12}$ in the clad layer of the sample treated at the scanning speed of 4 mm/s (Fig. 1) and its finer microstructure due to the faster cooling rate [22], as compared to the sample treated at 6 mm/s.

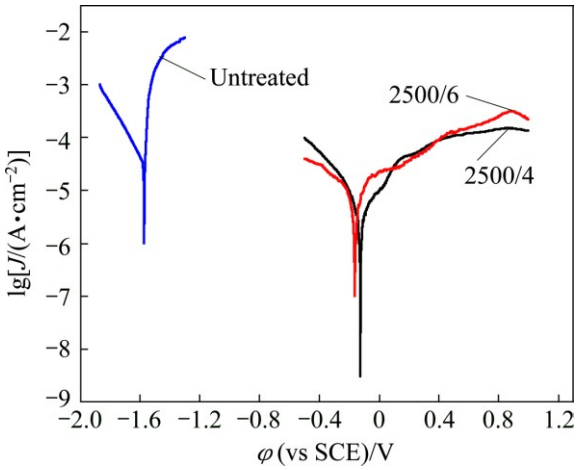

Fig. 5 Potentio-polarization curves of untreated and laser-clad Mg−6Zn−1Ca samples in 3.5% NaCl water solution

Table 2 φ_{corr} and J_{corr} values for untreated and laser-clad Mg−6Zn−1Ca in 3.5% NaCl water solution

Specimen	φ_{corr} (vs SCE)/mV	J_{corr}/(μA·cm^{-2})
Mg−6Zn−1Ca substrate	−1574.6	170.1
2500/4	−128.7	6.7
2500/6	−165.3	12.8

4 Conclusions

1) After the laser cladding treatment, XRD analysis shows that intermetallic phases, such as Mg_2Si, $Mg_{17}Al_{12}$ and Al_3Mg_2, are produced in the clad layer.

2) Due to the grain refinement and the presence of the intermetallic phases, the microhardness is significantly increased from $HV_{0.025}$ 54 for the substrate to $HV_{0.025}$ 310 for the laser-clad layer.

3) Corrosion resistance of the laser-clad specimens can be greatly improved compared with the substrate. In particular, the J_{corr} value of the laser-clad sample with the scanning speed of 4 mm/s is 6.7 μA/cm^2, much lower than that of the untreated sample (170.1 μA/cm^2). This is attributed to the grain refinement induced by rapid solidification and the increased Al content in the laser-clad layer compared with the substrate.

4) The results show that the depth of hardened layer increases and the corrosion resistance becomes better when the laser scanning speed is lower.

References

[1] JIANG J H, ZHOU Q, YU J S, MA A B, SONG D, LU F M. Comparative analysis for corrosion resistance of micro-arc oxidation coatings on coarse-grained and ultra-fine grained AZ91D Mg alloy [J]. Surfer and Coatings Technology, 2013, 216: 259−266.

[2] MIURA H, MARUOKA T, JONAS J J. Effect of ageing on microstructure and mechanical properties of a multi-directionally forged Mg−6Al−1Zn alloy [J]. Materials Science and Engineering A, 2013, 563: 5−9.

[3] LIU W J, CAO F H, JIA B L, ZHENG L Y, ZHANG J Q, CAO C N. Corrosion behavior of AM60 magnesium alloys containing Ce or La under thin electrolyte layers [J]. Corrosion Science, 2010, 52: 639−650.

[4] ZHEMCHUZHNIKOVA D, MOGUCHEVA A, KAIBYSHEV R. Mechanical properties and fracture behavior of an Al−Mg−Sc−Zr alloy at ambient and subzero temperatures [J]. Materials Science and Engineering A, 2013, 565: 132−141.

[5] GAO B, HAO S Z, ZOU J X, WU W, TU G F. Effect of high current pulsed electron beam treatment on surface microstructure and wear and corrosion resistance of an AZ91HP magnesium alloy [J]. Surface and Coatings Technology, 2007, 201: 6297−6303.

[6] LIU H X, XU Q. Corrosion resistance and mechanical property of AZ31 magnesium alloy by N/Ti duplex ion implantation [J]. Surface and Coatings Technology, 2013, 228: s538−s543.

[7] YANG J X, CUI F Z. Plasma surface modification of magnesium alloy for biomedical application [J]. Surface and Coatings Technology, 2010, 205: s182−s187.

[8] SAMEER R P, ANANYA B. Improved corrosion and wear resistance of Mg alloys via laser surface modification of Al on AZ31B [J]. Surface and Coatings Technology, 2012, 206: 2308−2315.

[9] SURMENEVA M A, SURMENEV R A. Microstructure characterization and corrosion behaviour of a nanohydroxyapatite coating deposited on AZ31 magnesium alloy using radio frequency magnetron sputtering [J]. Vacuum, 2015, 117: 60−62.

[10] BAKIN B, DELICE T K, TIRIC U, BIRLIK I, AZEM F A. Bioactivity and corrosion properties of magnesium-substituted CaP coatings produced via electrochemical deposition [J]. Surface and Coatings Technology, 2016, 301: 29−35.

[11] CUI Xue-jun, YANG Rui-song, LIU Chun-hai, YU Zu-xiao, LIN Xiu-zhou. Structure and corrosion resistance of modified micro-arc oxidation coating on AZ31B magnesium alloy [J]. Transactions of Nonferrous Metals Society of China, 2016, 26: 814−821.

[12] QIAN J G, ZHANG J X. Study on laser cladding $NiAl/Al_2O_3$ coating on magnesium alloy [J]. Rare Metal Materials and Engineering, 2013, 42: 466−469.

[13] YUE T M, XIE H. Solidification behaviour in laser cladding of AlCoCrCuFeNi high-entropy alloy on magnesium substrates [J]. Journal of Alloys and Compounds, 2014, 587: 588−593.

[14] HAZRA M, MONDAL A K. Laser surface cladding of MRI 153M magnesium alloy with ($Al+Al_2O_3$) [J]. Surface and Coatings Technology, 2009, 203: 2292−2299.

[15] CAO X, JAHAZI M. Optimization of bead spacing during laser cladding of ZE41A-T5 magnesium alloy castings [J]. Journal of Materials Processing Technology, 2008, 205: 322−331.

[16] TAN C L, ZHU H M, KUANG T C, SHI J, LIU H W, LIU Z W. Laser cladding Al-based amorphous-nanocrystalline composite coatings on AZ80 magnesium alloy under water cooling condition [J]. Journal of Alloys and Compounds, 2017, 690: 108−115.

[17] WANG C S, LI T. Laser cladding of eutectic-based Ti−Ni−Al alloy coating on magnesium surface [J]. Surface and Coatings Technology, 2010, 205: 189−194.

[18] WANG J F, WEI Y Y. The Y-doped MgZnCa alloys with ultrahigh specific strength and good corrosion resistance in simulated body fluid [J]. Materials Letters, 2012, 81: 112−114.

[19] LIU D X, GUO C G. Mechanical properties and corrosion resistance of hot extruded Mg−2.5Zn–1Ca alloy [J]. Materials Science and Engineering B, 2015, 195: 50−58.

[20] YANG Y, WU H. Improving the wear resistance of AZ91D magnesium alloys by laser cladding with Al−Si powders [J]. Materials Letters, 2009, 63: 19−21.

[21] WANG A H, YUE T M. YAG laser cladding of an Al-Si alloy onto an Mg/SiC composite for the improvement of corrosion resistance [J]. Composites Science and Technology, 2001, 61: 1549−1554.

[22] CHEN E L, ZHANG K M, ZOU J X. Laser cladding of a Mg based Mg−Gd−Y−Zr alloy with Al−Si powders [J]. Applied Surface Science, 2016, 367: 11−18.

[23] WEN Y, SUN R L, TANG Y. Experimental and thermodynamic investigations into the microstructure of laser clad Al−Si coatings on AZ91D alloys [J]. Surface and Coatings Technology, 2012, 207: 400−405.

[24] YANG Y, WU H. Improving the wear resistance of AZ91D magnesium alloys by laser cladding with Al−Si powders [J]. Materials Letters, 2009, 63: 19−21.

[25] LUNDER O, LEIN J E, AUNE T K, NISANCIOGLU K. The role of $Mg_{17}Al_{12}$ phase in the corrosion of Mg alloy AZ91 [J]. Corrosion, 1989, 45: 741−748.

[26] LU Y, BRADSHAW A R, CHIU Y L, JONES I P. Effects of secondary phase and grain size on the corrosion of biodegradable Mg−Zn−Ca alloys [J]. Materials Science and Engineering C, 2015, 48: 480−486.

Mg−6Zn−1Ca 合金激光熔覆 Al−Si 层的组织与性能

张晓林[1]，张可敏[1]，邹建新[2]

1. 上海工程技术大学 材料工程学院，上海 201620；
2. 上海交通大学 材料科学与工程学院 轻合金精密成型国家工程研究中心，上海 200240

摘 要：采用激光熔覆 Al−Si 粉体以提高 Mg−6Zn−1Ca 合金的表面性能，并采用 X 射线衍射(XRD)、扫描电镜(SEM)和能谱(EDS)技术研究熔覆层的相组成、组织结构和化学成分。结果表明，熔覆层主要由 α-Mg、Mg_2Si 枝晶、$Mg_{17}Al_{12}$ 和 Al_3Mg_2 相组成。由于生成了 Mg_2Si、$Mg_{17}Al_{12}$ 和 Al_3Mg_2 金属间化合物以及快速熔凝的晶粒细化作用，熔覆层的显微硬度($HV_{0.025}$ 310)比基体硬度($HV_{0.025}$ 54)高近 5 倍。同时，在 3.5% NaCl(质量分数)水溶液中的腐蚀性能测试显示，腐蚀电位从基体的−1574.6 mV 上升到了熔覆后的−128.7 mV，而腐蚀电流密度则从基体的 170.1 μA/cm^2 降至熔覆后的 6.7 μA/cm^2。这些研究结果显示，激光熔覆 Al−Si 粉体可以显著提高 Mg−6Zn−1Ca 合金表层的硬度和耐蚀性。

关键词：激光熔覆；Mg−6Zn−1Ca 合金；显微组织；硬度；耐蚀性

(Edited by Bing YANG)